ACCOUNTS of chemical research

pubs.acs.org/accounts Article

# Selectivity by the Clock: Programming Reactivity with Alternating Current Frequency

*Published as part of Accounts of Chemical Research special issue "Globalizing Electroorganic Synthesis".*

Diptangshu Datta Mal,[‡] Nibedita Behara,[‡] and Long Luo*

Cite This: https://doi.org/10.1021/acs.accounts.6c00439 Read Online

ACCESS | Metrics & More | Article Recommendations



**CONSPECTUS:** Electrochemical reactions are inherently programmable through the applied potential. However, conventional direct current (DC) electrolysis provides only limited control over reaction selectivity because it generates a static redox environment in which substrates and intermediates remain continuously exposed to either oxidizing or reducing conditions. As a result, reactive intermediates often undergo undesired overoxidation, overreduction, or competing side reactions. Alternating current (AC) electrolysis overcomes these limitations by periodically reversing electrode potential polarity, creating a dynamic redox environment in which oxidation and reduction can be regulated in the time domain. In addition to potential, AC electrolysis introduces frequency as a new experimental parameter for controlling reaction pathways. In this Account, we highlight our group's recent efforts to understand how AC frequency controls reaction selectivity. We show that AC frequency serves as a kinetic synchronization parameter, matching electrochemical time scales to the rates of key chemical steps. By controlling the duration that reactive intermediates experience oxidizing or reducing environments, AC electrolysis enables selective access to reaction pathways that are difficult or impossible to achieve under conventional DC conditions. Using representative examples, we illustrate several mechanistic modes through which AC frequency governs reaction outcomes. First, we demonstrate that frequency-controlled modulation of the redox environment can distinguish between one- and two-electron oxidation pathways of amines, enabling the selective generation of $\alpha$-amino radicals while suppressing the formation of iminium ions. This principle was further extended to electrochemical hydrogen isotope exchange, in which AC frequency synchronizes proton transfer and hydrogen atom transfer to achieve efficient, site-selective isotope incorporation. Second, we show that AC frequency can synchronize with homogeneous catalytic cycles. In a Ni-catalyzed C−N cross-coupling reaction, the optimal frequency arises from matching the AC waveform to the formation rate of a key Ni(II) catalytic resting state. Third, we demonstrate that AC electrolysis can dynamically maintain catalytically active electrode structures and alter chemical speciation in heterogeneous electrocatalysis. In an industrial Ag-catalyzed dehalogenation process, AC electrolysis continuously regenerates a defect-rich Ag catalyst while suppressing chlorine-mediated decomposition pathways, leading to dramatically improved long term selectivity and catalyst stability. We further describe our efforts to establish finite-element modeling approaches for AC electrolysis. Using the AC-enabled partial reduction of (hetero)arenes as a model system, we show how electrochemical kinetics extracted from cyclic voltammetry can be integrated with finite-element simulations to reproduce experimental selectivity trends and identify the kinetic criteria required for selective partial reduction. These studies demonstrate that quantitative modeling can provide mechanistic insight and guide reaction design. Collectively, these examples reveal a unifying principle: AC electrolysis enables control of chemical reactivity by synchronizing electrochemical inputs with the intrinsic time scales of key selectivity determining chemical/electrochemical processes. Although significant challenges remain in developing predictive models for complex reactions, we envision that continued advances in electroanalytical methods, mechanistic studies, and computational modeling will transform AC electrolysis from an empirical optimization tool into a general strategy for programming reaction selectivity through temporal control

*continued...*

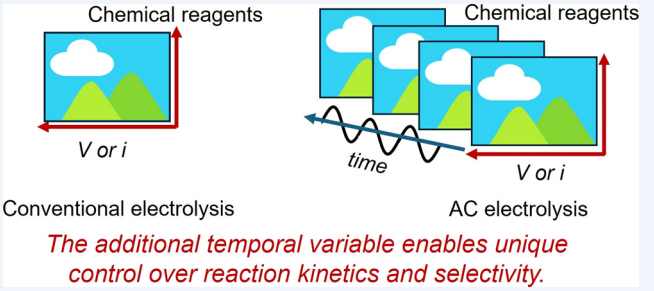


Received: June 4, 2026
Revised: July 1, 2026
Accepted: July 6, 2026

of the electrochemical environment.

## KEY REFERENCES

- Gunasekera, D.; Mahajan, J. P.; Wanzi, Y.; Rodrigo, S.; Liu, W.; Tan, T.; Luo, L. Controlling One- or Two-Electron Oxidation for Selective Amine Functionalization by Alternating Current Frequency. *J. Am. Chem. Soc.* **2022**, *144* (22), 9874−9882.[1] This paper demonstrates that the AC electrolysis frequency can be used to selectively direct one- or two-electron amine oxidation toward amino radicals or iminium cations, enabling controllable $\alpha$-amine arylation or cyanation. Cyclic voltammetric analysis was used to predict the optimal frequency.
- Behera, N.; Gunasekera, D.; Mahajan, J. P.; Frimpong, J.; Liu, Z. F.; Luo, L. Electrochemical Hydrogen Isotope Exchange of Amines Controlled by Alternating Current Frequency. *Faraday Discuss.* **2023**, *247*, 45−58.[2] This paper describes the first electrochemical protocol for hydrogen isotope exchange and, via kinetic analysis, provides a quantitative understanding of the optimal frequency for H/D exchange at the $\alpha$-amino sites of tetrahydroisoquinolines and pyrrolidines.
- Sreekumar, S.; Beeler, J. A.; Mal, D. D.; White, H. S.; Luo, L. Origin of Selectivity in Alternating Current-Enabled Partial Reduction of (Hetero)Arenes: A Case Study of Two Consecutive Irreversible Electrochemical Steps. *J. Am. Chem. Soc.* **2025**, *147* (30), 26917−26925.[3] This paper uncovers the origin of selectivity in AC-enabled partial reduction of (hetero)arenes to cyclic alkenes, a model reaction involving two consecutive irreversible electrochemical steps, through fast-scan voltammetry and finite-element simulations.
- Hazra, A.; Organiscak, M.; Luo, L. Deciphering the Synchronization of Alternating Current Frequency with the Nickel Catalytic Cycle in Selective C-N Cross-Coupling. *J. Am. Chem. Soc.* **2025**, *147* (38), 35139−35148.[4] This paper uncovers how AC frequency synchronizes with key steps in a Ni-catalyzed cross-coupling cycle to control product selectivity between C−N and C−C coupling.
- Mal, D. D.; Redkar, N.; Liu, K.; Park, H.; Kennedy, E. R.; Kim, S.; Li, W.; Yang, Y.; Qi, Y.; Neurock, M. Electrosynthesis of Agrochemicals via Alternating-Current-Driven Selective, Continuous Dehalogenation. *J. Am. Chem. Soc.* **2025**, *147* (41), 37611−37621.[5] This work showcases an AC electrolysis strategy that maintains the active silver catalyst structure and controls reactive solution species to suppress undesired deamination and decomposition reactions during continuous dechlorination.

## 1. INTRODUCTION

Controlling reaction selectivity is a long-standing challenge in organic synthesis because multiple competing reaction pathways, intermediates, and products often coexist under similar reaction conditions.[6,7] Achieving high selectivity requires precise control over the reactivity of these chemical species to favor the desired transformation while suppressing undesired ones. This challenge becomes even more significant in complex molecular systems containing multiple reactive functional groups or chemically similar reaction sites.[8−10] Therefore, the development of strategies that enable predictable and tunable control over chemo-, regio-, and stereoselectivity remains a central goal in modern synthetic chemistry.

The conventional approach to controlling reaction selectivity has primarily focused on the development and utilization of new chemical reagents, including the design of specialized chemicals,[11,12] catalysts,[13,14] ligands,[15,16] solvents,[17,18] and additives[19,20] that can selectively favor one reaction pathway over another. In transition-metal catalysis, for example, carefully engineered ligands are often employed to tune the steric and electronic environment around the metal center, thereby modulating the reactivity and selectivity of key catalytic intermediates.[21,22] Similarly, the use of directing groups, protecting groups, or tailored oxidants and reductants has enabled chemists to achieve improved chemo-, regio-, and stereoselectivity in a wide range of transformations.[23,24] These approaches have significantly advanced the field of synthetic chemistry and enabled many previously inaccessible reactions. However, they often require extensive optimization and the synthesis of specialized chemicals, thereby increasing the complexity and cost of reaction development.

Recently, electroorganic synthesis has been experiencing a strong renaissance in modern synthetic chemistry.[25,26] The driving force behind this resurgence is not only that electrochemistry represents a more sustainable synthetic approach, in which electrons are used directly as redox reagents to drive chemical transformations, but also its unique ability to control reaction pathways and selectivity through electrochemical parameters.[27,28] Unlike conventional synthetic methods that primarily rely on modifying the chemical composition of the reaction system, electroorganic synthesis introduces additional dimensions of control, including applied potential/current density, electrolyte composition, and electrode materials.[29] Among these parameters, the applied potential or current can selectively access specific redox-active intermediates by controlling the thermodynamics and kinetics of electron-transfer processes.[30] At the same time, the choice of electrolyte and electrode materials can strongly influence interfacial interactions and, thus, the stability of reactive intermediates.[31,32] As a result, electrochemical methods can enable selective activation of substrates and provide access to reaction pathways that are difficult or inaccessible using conventional chemical reagents.

Conventional electroorganic synthesis typically relies on applying a constant current or constant potential (i.e., DC electrolysis) to drive electrochemical transformations. Under these static operating conditions, substrates and intermediates are continuously exposed to either oxidizing or reducing environments throughout the reaction.[25] As a consequence, reactions conducted under DC electrolysis often favor the formation of thermodynamically stable products rather than kinetically controlled ones. Reactive intermediates or products generated at the electrode surface may undergo additional electron-transfer steps before diffusing away from the interface, leading to undesired overoxidation or overreduction processes.[33] In such systems, maintaining selective access to transient intermediates while preventing subsequent undesired electrochemical reactions is often difficult under DC electrolysis.[34] Therefore, developing strategies that dynamically modulate the electrochemical environment, such as alternating


https://doi.org/10.1021/acs.accounts.6c00439
Acc. Chem. Res. XXXX, XXX, XXX−XXX

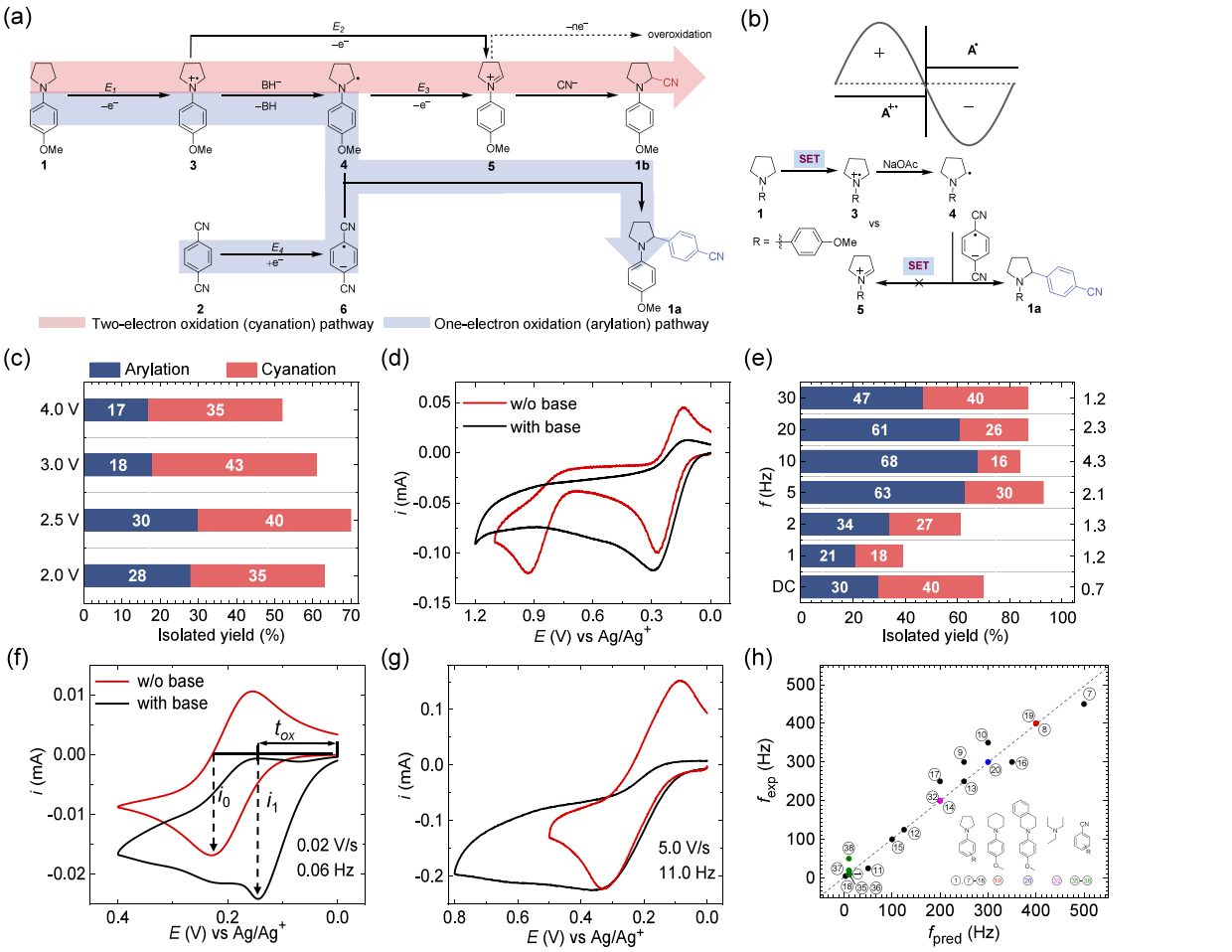


**Figure 1.** (a) One- and two-electron oxidation pathways in electrochemical $\alpha$-amino C−H functionalization leading to arylation product **1a** and cyanation product **1b**. (b) Proposed mechanism behind the AC frequency-controlled one- vs two-electron oxidation of amines. (c) Effect of cell voltage on the yields of arylation and cyanation products under DC electrolysis. (d) CV of **1** with (black) and without (red) NaOAc. (e) Isolated yields of arylation and cyanation products at varying AC frequencies from 1 to 30 Hz. (f) and (g) CVs of **1** in the presence and absence of NaOAc base at (f) 0.02 V/s and (g) 5.0 V/s. (h) Plot of experimentally determined optimal frequencies ($f_{exp}$) vs CV-predicted optimal frequencies ($f_{pred}$) for various tertiary amines and cyanoaromatics. Reproduced with permission from ref 1. Copyright 2022 American Chemical Society.

current (AC) electrolysis, has emerged as an attractive approach for improving reaction selectivity and accessing nonequilibrium reaction pathways.[35,36]

Over the past decade, multiple research groups, including those led by Hilt, Semenov, Lei, Baran, Malapit, Hibino, He, De Bon, Zhu, and our own, have demonstrated the power of AC electrolysis to control reaction pathways and improve synthetic outcomes. Early studies from Hilt's group showed that AC electrolysis could prevent overoxidation and overreduction in sulfur−sulfur bond metathesis reactions and enable acyl nitroso Diels−Alder cycloadditions.[37,38] Semenov and co-workers subsequently demonstrated that AC electrolysis could enhance both the efficiency and scalability of Ni-catalyzed transformations.[39,40] Lei's group employed AC electrolysis to mitigate catalyst deposition issues and developed a range of C−H functionalization reactions.[42−45] Baran and co-workers expanded the synthetic scope of AC electrolysis by developing chemoselective reductions of (hetero)arenes and phthalimides,[48,49] as well as Kolbe reactions[41] and decarboxylative coupling processes.[51] Malapit and co-workers further applied AC electrolysis to aryl C−P bond formation[46] and olefin hydrocarboxylation.[47] Beyond electroorganic synthesis, He and co-workers utilized pulsed electrolysis to promote cascade reaction sequences for C−N bond formation.[50] De Bon and co-workers demonstrated enhanced control over atom transfer radical polymerization of acrylates using AC electrolysis,[54] whereas Zhu and co-workers integrated AC electrolysis with paired photoelectrocatalysis to achieve asymmetric alcohol cross-coupling.[52] Alongside these efforts, our group has explored AC electrolysis across a broad range of transformations, including trifluoromethylation of (hetero)arenes,[53] selective amine functionalization,[1] hydrogen isotope exchange of amines,[2] functional-group-tolerant alkene difunctionalization,[55] selective Ni-catalyzed C−N coupling,[4] heterogeneous Ag-catalyzed dehalogenation,[5] and stereoselective electroenzymatic H/D exchange reactions.[56]

In addition to the rapid expansion of AC-enabled synthetic methodologies, significant efforts have also been devoted to understanding the origins of AC-controlled selectivity. To this end, Yuen-Zhou and co-workers,[57−59] Malapit and co-workers,[60] Chen and co-workers,[34] and our group[3] have developed theoretical, computational, and analytical (including voltammetry and mass spectrometry) frameworks that provide mechanistic insights into AC-driven reaction pathways and guide the rational design of future AC electrochemical transformations.


https://doi.org/10.1021/acs.accounts.6c00439
Acc. Chem. Res. XXXX, XXX, XXX−XXX

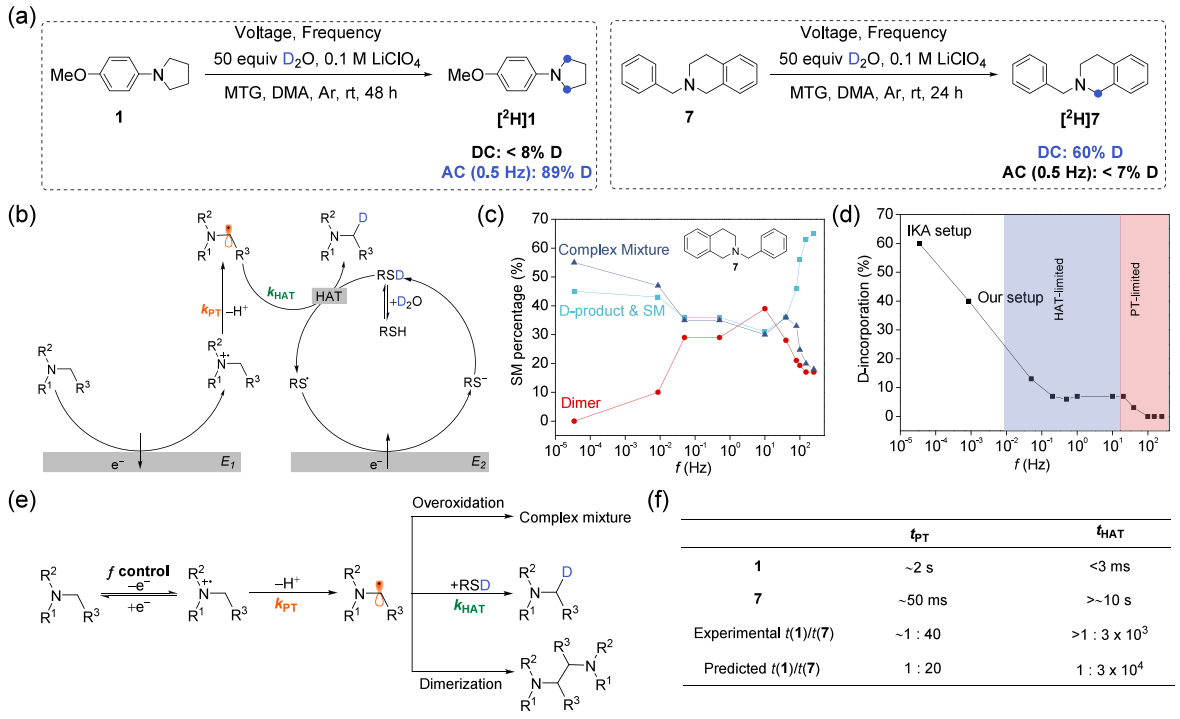


| | $t_{PT}$ | $t_{HAT}$ |
|---|---|---|
| **1** | ~2 s | <3 ms |
| **7** | ~50 ms | >~10 s |
| Experimental $t$(**1**)/$t$(**7**) | ~1 : 40 | >1 : 3 x $10^3$ |
| Predicted $t$(**1**)/$t$(**7**) | 1 : 20 | 1 : 3 x $10^4$ |

**Figure 2.** (a) Electrochemical HIE of pyrrolidine (**1**) and tetrahydroisoquinoline (**7**) under AC and DC conditions. (b) Proposed mechanism of electrochemical HIE. Frequency-dependent (c) product analysis and (d) D-incorporation of **7**. (e) Schematic representation of frequency-controlled pathways for the formation of the D-labeled amine, dimer, and overoxidized products. (f) Estimated time scale for deprotonation ($t_{PT}$) and HAT ($t_{HAT}$) for **1** and **7**. Reproduced with permission from ref 2. Copyright 2023 Royal Society of Chemistry.

In this Account, we highlight our group's contributions in the development of AC electrolysis for organic synthesis through several representative examples. These studies span a broad range of reaction classes, from controlling the reactivity of radical intermediates to synchronizing AC electrolysis with homogeneous catalysis and heterogeneous catalysis. We also discuss how identifying the key elementary steps that interact with the alternating redox environment has enabled frequency-dependent control over reaction selectivity and efficiency. Finally, we provide our perspective on the future opportunities and challenges for this rapidly evolving field.

## 2. CONTROLLING THE REACTIVITY OF AMINO RADICAL SPECIES

As mentioned earlier, when multiple reaction intermediates could coexist in a reaction mixture, DC electrolysis often favors the thermodynamically stable ones. One example is amine functionalization. Amines can undergo one-electron oxidation to form amine cation radicals or amino radicals, or two-electron oxidation to iminium.[61−63] Under DC electrolysis, the amine substrate is prone to being oxidized to an iminium cation, which can then be trapped by nucleophiles. This reaction is the classical Shono oxidation, one of the most influential transformations in organic electrochemistry. Limiting amine oxidation to a one-electron process is more challenging because the resulting amino radical is more readily oxidized than the parent amine. Consequently, it is rapidly converted to the corresponding iminium ion under conventional electrochemical conditions, making selective access to amino radical pathways difficult.

Figure 1a shows a model electrochemical amine functionalization reaction demonstrating the competition between these two amine oxidation pathways. The pyrrolidine substrate, **1**, undergoes electrochemical oxidation, and the 1,4-dicyanobenzene **2** undergoes one-electron reduction to radical anion **6**. The one-electron oxidation of amine **1** leads to the amine radical cation **3**, followed by deprotonation to deliver the $\alpha$-amino radical **4**. Further oxidation of amine radical **4** leads to iminium cation **5**. The radical−radical reaction between radical **4** and the radical anion **6** yields the arylated product **1a** after the elimination of $CN^-$. While the two-electron oxidation intermediate, the iminium cation, **5**, undergoes nucleophilic addition with $CN^-$, leading to the cyanation byproduct **1b**.

Under DC conditions, varying the applied voltage did not improve the selectivity for the arylated product relative to the cyanation product, suggesting that two-electron oxidation of the amine is unavoidable (Figure 1c). Cyclic voltammograms (CV) of amine **1** in the presence and absence of NaOAc further supports this conclusion (Figure 1d). In the absence of NaOAc, the voltammogram shows two distinct anodic peaks. The first peak at $E_1 \approx 0.3$ V vs $Ag/Ag^+$ corresponds to the reversible single-electron oxidation of amine **1** to radical cation **3**, whereas the second peak at $E_2 \approx 0.9$ V is assigned to further oxidation to iminium cation **5**. In the presence of NaOAc, however, the second peak shifts to a lower potential and merges with the first peak, accompanied by an increase in current. This behavior indicates that one- and two-electron oxidation of **1** occurs concurrently at lower potentials. As a result, the arylation product is consistently formed together with the cyanation product under DC conditions.

Interestingly, we found that the selectivity between the arylation and cyanation pathways could be readily controlled by adjusting the AC frequency. As shown in Figure 1e, increasing the frequency from 1 to 30 Hz shifted the product distribution towards the arylated product. The highest selectivity was achieved at 10 Hz, affording the arylated and cyanation products in yields of 68% and 16%, respectively. This frequency-


https://doi.org/10.1021/acs.accounts.6c00439
Acc. Chem. Res. XXXX, XXX, XXX−XXX

dependent selectivity effectively overcomes the selectivity limitation observed in DC electrolysis.

To gain mechanistic insight into the frequency-dependent product selectivity, we performed CV experiments at varying scan rates and analyzed the relationship between peak current and scan rate. The rationale is that the scan rate serves as a proxy for the reaction time scale, analogous to the frequency in AC electrolysis, while the peak current reflects the extent of amine oxidation. In general, the greater the number of electrons removed from the amine, the larger the oxidation current. Therefore, by examining how the peak current changes with scan rate, it is possible to probe the relative contributions of competing amino radical and iminium pathways occurring on different time scales.

The red curves in Figures 1f and 1g show the CVs of amine **1** in the absence of NaOAc at scan rates of 0.02 and 5 V/s, respectively. Under these conditions, the voltammograms represent a reversible one-electron redox process, and the corresponding anodic peak currents ($i_0$) were therefore used as references for single-electron oxidation. At a slow scan rate of 0.02 V/s, the addition of NaOAc significantly increases the anodic peak current ($i_1$) relative to $i_0$, indicating that NaOAc promotes further oxidation of **1** through deprotonation of radical cation **3** and subsequent formation of the iminium species. In contrast, at a scan rate of 5 V/s, $i_1$ becomes nearly identical to $i_0$, suggesting that only one-electron oxidation occurs on this time scale, even in the presence of NaOAc.

The time required to scan from the oxidation onset potential to the anodic peak potential at 5 V/s is approximately 45 ms ($t_{ox} \approx 45$ ms). This time scale represents the maximum duration during which radical cation **3** can persist without undergoing significant deprotonation and further oxidation. Converting this oxidation duration to an equivalent AC frequency using our formula $f = 1/(2t_{ox})$ yields approximately 11 Hz, which is in excellent agreement with the experimentally observed optimum frequency of 10 Hz. This correlation suggests that the enhanced selectivity arises from synchronization of the redox environment with the kinetics of amine cation radical deprotonation through frequency tuning (Figure 1b). At the optimal frequency, the electrode potential reverses before radical cation **3** can undergo deprotonation and subsequent overoxidation. Instead, **3** is deprotonated to generate $\alpha$-amino radical **4** during the following negative pulse, which allows effective radical−radical coupling to afford the desired arylation product **1a** rather than being converted to the iminium intermediate that leads to cyanation. Using the CV method, we examined a series of amines and found that the CV-predicted optimal frequencies ($f_{pred}$) closely matched the experimentally determined ones ($f_{exp}$; Figure 1h).

A particularly exciting finding from Figure 1h is that different amines exhibit dramatically different optimal frequencies for $\alpha$-amino radical formation, spanning more than 3 orders of magnitude. This observation suggested that AC frequency could potentially serve as a unique kinetic parameter for selectively activating specific amine functionalities in a complex molecule based on their intrinsic oxidation and deprotonation kinetics.

To test our idea, we selected hydrogen isotope exchange (HIE) of amines as a model reaction because it proceeds via the same $\alpha$-amino radical intermediates as the arylation reaction.[2] As illustrated in Figure 2b, the electrochemical HIE process involves three key steps: (i) oxidation of the amine to generate an amine radical cation, (ii) proton transfer (PT) to form the corresponding $\alpha$-amino radical, and (iii) hydrogen atom transfer (HAT) from a deuterated thiol to the $\alpha$-amino radical, affording the D-labeled amine and a thiyl radical. The resulting thiyl radical is subsequently reduced electrochemically to regenerate the thiol catalyst, thereby completing the catalytic cycle.

To evaluate the effect of AC frequency on HIE reactivity, we selected two model amine substrates, pyrrolidine (**1**) and tetrahydroisoquinoline (**7**), because they exhibit markedly different optimal frequencies for $\alpha$-amino radical formation according to Figure 1h.

Consistent with our hypothesis, the two substrates indeed displayed dramatically different frequency-dependent HIE behavior (Figure 2a). **1** achieved its highest D-incorporation at 0.5 Hz, whereas **7** performed best under DC electrolysis conditions. We analyzed the product distributions of **1** and **7** for electrochemical HIE at different frequencies. Figure 2c shows that the dimer product is dominant in the higher-frequency range of 0.1 to 10 Hz for **7**, and the starting material is mostly recovered at frequencies above 10 Hz. Unlike **7**, **1** undergoes overoxidation at $f < 0.1$ Hz, leading to a complex mixture, and shows similar D-incorporation from 0.1 to 300 Hz. This product analysis reveals that $\alpha$-amino radical can undergo three possible competing pathways: HAT with deuterated thiol, homodimerization, and overoxidation, which collectively determine the efficiency of D-incorporation (Figure 2e).

Successful D-incorporation requires that the amine radical cation undergo PT and subsequent HAT before being consumed by competing pathways. The time scale of the PT step ($t_{PT}$) can be estimated from the frequency at which significant recovery of the unlabeled starting amine is observed. For **7**, this transition occurs at approximately 20 Hz (Figures 2c and 2d), corresponding to a characteristic PT time scale of ∼50 ms. Applying the same analysis to **1** yields a $t_{PT}$ value of approximately 2 s.

The time scale of the HAT step ($t_{HAT}$) can be inferred from the highest frequency at which substantial D incorporation starts. For **1**, high D-incorporation was maintained even at 300 Hz, the highest frequency examined in this study, indicating that HAT occurs within less than 3 ms. In contrast, efficient labeling of **7** was observed only under DC electrolysis conditions. Given that the diffusion time between the anode and cathode is on the order of 10 s under our reaction conditions, the HAT process for **7** is expected to occur on a comparable time scale. The relative PT and HAT time scales for **1** and **7** are consistent with the trends predicted from CV and bond dissociation energy analyses, respectively (Figure 2f). These results demonstrate that AC electrolysis can serve as a kinetic probe for dissecting the elementary steps of electrochemical HIE reactions and provide a mechanistic basis for the distinct optimal frequencies observed for different amine substrates.

Encouraged by the initial success of electrochemical HIE on simple amines, we next explored the feasibility of applying this method to the site-selective labeling of pharmaceutical compounds. This goal proved challenging because the majority of amine functionalities in drug molecules are alkyl amines, whose corresponding $\alpha$-amino radicals are significantly less stabilized than those derived from aryl amines. As a result, efficient HAT and D-incorporation are considerably more difficult to achieve.

Most recently, we addressed this challenge by discovering a new HAT catalyst, 1,3-propanedithiol.[64] Using this catalyst, electrochemical HIE was successfully extended to alkyl amine-containing pharmaceuticals under AC electrolysis conditions. The exceptional performance of 1,3-propanedithiol stems from its ability to generate a highly reactive mercaptothiyl radical with


https://doi.org/10.1021/acs.accounts.6c00439
Acc. Chem. Res. XXXX, XXX, XXX−XXX

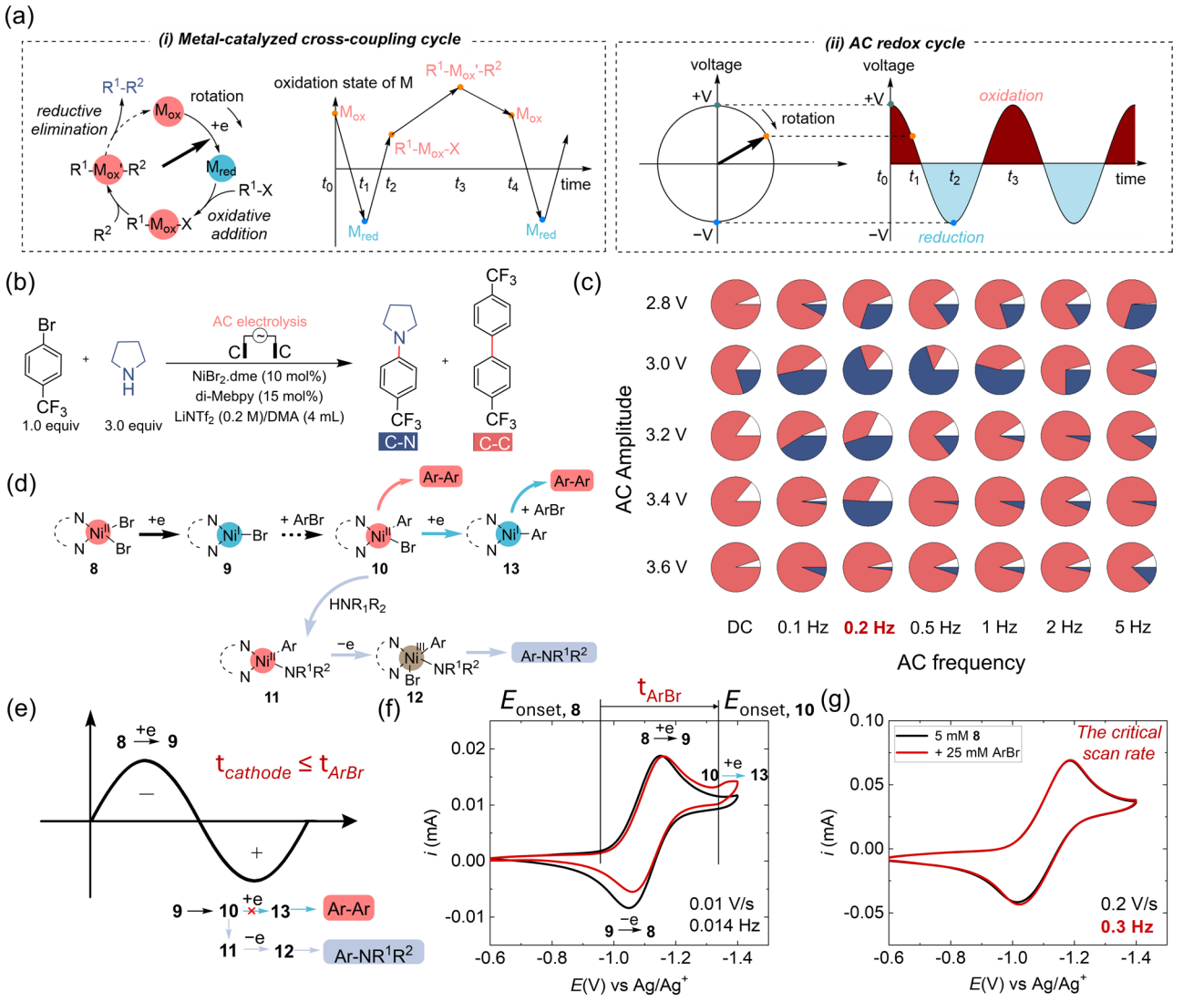


**Figure 3.** (a) Schematic illustration of the similar periodicity of a metal-catalyzed cross-coupling catalytic cycle with an AC-driven redox cycle. (b) Representative reaction scheme for the coupling of an aryl bromide (ArBr) with an amine, yielding C−N and C−C coupled products, denoted by blue and pink, respectively. (c) Product selectivity as a function of AC amplitude and frequency, highlighting that selective C−N coupling is favored at 3 V and 0.2 Hz. (d) Proposed overall mechanism outlining the electrochemical and chemical steps leading to both C−N and C−C bond formation. The dashed arrow from **9** to **10** represents multiple chemical steps. (e) Schematic depiction of temporal alignment between the applied AC sine waveform and key steps in the simplified reaction mechanism. At the optimal frequency for selective C−N coupling, the cathodic half-cycle duration ($t_{cathode}$) is comparable to or shorter than the oxidative addition time scale ($t_{ArBr}$). (f) CVs of the Ni(II)-di-Mebpy catalyst recorded in the absence (black trace) and presence (red trace) of ArBr at a scan rate of 0.01 V/s, showing the **8** → **9** and **10** → **13** reduction processes. The oxidative addition time scale ($t_{ArBr}$) was estimated from the onset potentials of these reductions and the scan rate. (g) CVs obtained at a critical scan rate of 0.2 V/s, where the **10** → **13** reduction is suppressed, and the two voltammograms overlap. Reproduced with permission from ref 4. Copyright 2025 American Chemical Society.

an unusually low effective S−H bond dissociation energy of approximately 34 kcal mol$^{-1}$, compared with ∼80 kcal mol$^{-1}$ for conventional monothiols. This dramatic reduction originates from the favorable formation of a 5-membered disulfide ring upon the loss of a hydrogen atom via HAT, which provides a strong thermodynamic driving force for the HAT process. Combined mechanistic, electrochemical, and computational studies further revealed that 1,3-propanedithiol possesses an optimal molecular architecture that balances rapid HAT with efficient catalyst regeneration, making it uniquely suited for electrochemical isotope-labeling applications.

## 3. SYNCHRONIZATION OF HOMOGENEOUS Ni CATALYSIS WITH AC ELECTROLYSIS

In parallel with our efforts to control amine-radical reactivity using AC electrolysis, we began exploring a second research direction focused on synchronizing homogeneous catalytic cycles with the applied AC wave. Both AC electrolysis and homogeneous catalytic cycles are inherently periodic processes: the electrode potential oscillates with time, while catalytic intermediates are generated and consumed in a cyclic manner (Figure 3a). This similarity led us to ask how these two periodic processes interact when operating on comparable time scales. A similar concept of resonant catalysis was also proposed by Dauenhauer and co-workers for heterogeneous catalytic systems.[65,66]


https://doi.org/10.1021/acs.accounts.6c00439
Acc. Chem. Res. XXXX, XXX, XXX−XXX

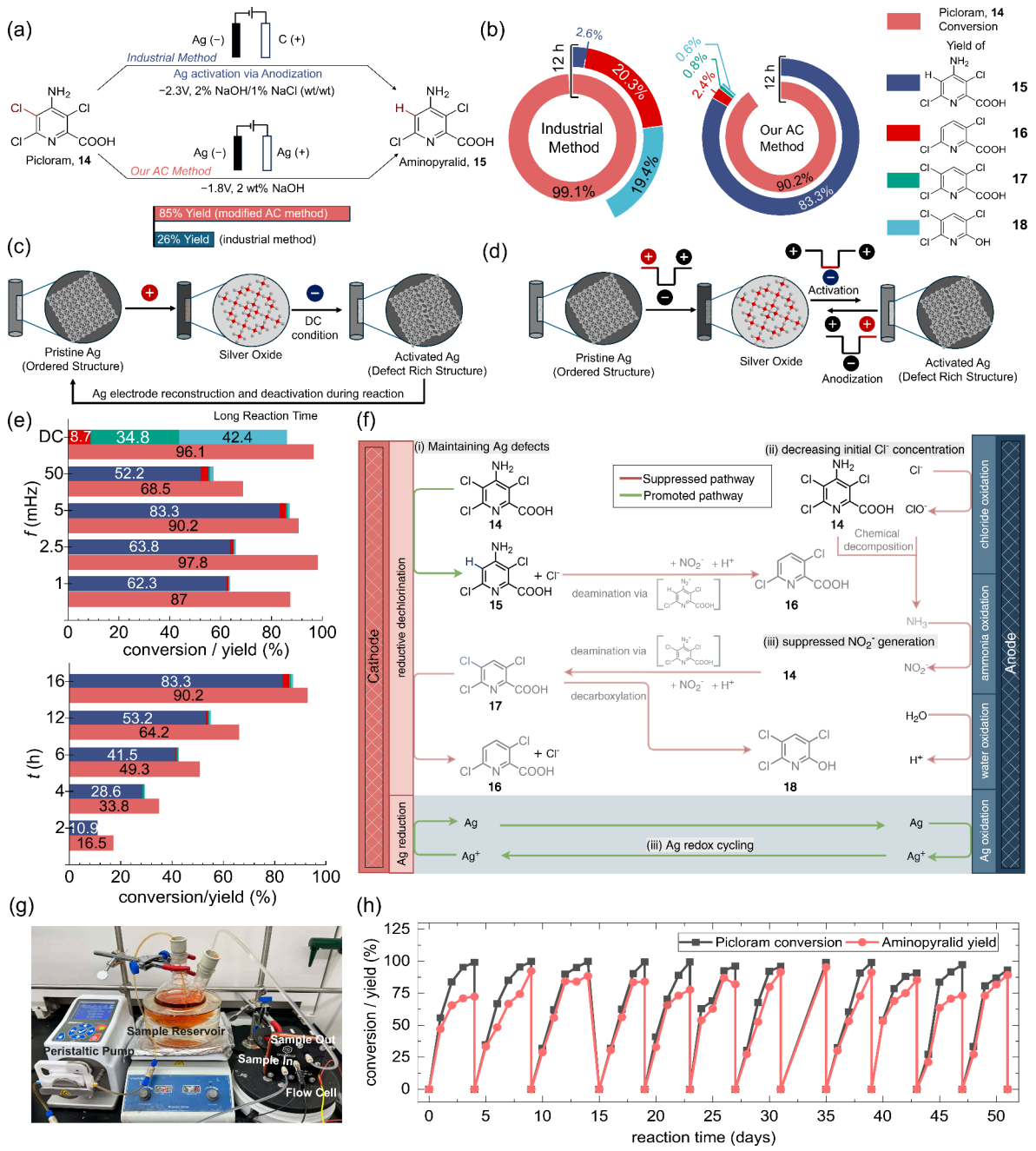


**Figure 4.** (a) Comparison of the industrial method and the proposed AC method for Ag-catalyzed dehalogenation of picloram (**14**). The AC method achieves an 85% yield of the desired product, aminopyralid (**15**), compared to 26% with the industrial method. (b) Product distribution for the industrial method and our AC method; in the industrial method, several deaminated byproducts (**16**, **17**, and **18**) are identified (listed on the right). (c) and (d) Evolution of Ag catalyst structure using (c) the industrial method and (d) our AC method. (e) Optimization of frequency and reaction time for the AC method. (f) Proposed reaction pathways under AC conditions, with suppressed pathways indicated in gray. (g) Flow-cell setup for large-scale synthesis. (h) Conversion of picloram and yield of aminopyralid in a continuous flow cell over 50 days. Reproduced with permission from ref 5. Copyright 2025 American Chemical Society.

We chose a Ni-catalyzed C−N cross-coupling reaction as our model system, inspired by the pioneering work of Semenov and co-workers on AC-enhanced Ni-catalyzed cross-coupling transformations.[39] Their studies demonstrated that AC electrolysis can significantly improve yields of desired cross-coupling products, compared with conventional DC electrolysis. In our study, we slightly modified the reported reaction conditions by replacing LiBr with $LiNTf_2$ and employing 6,6′-dimethyl-2,2′-bipyridine (di-Mebpy) instead of 4,4′-di-*tert*-butyl-2,2′-bipyridine (di-tBubpy) as the ligand. The removal of high concentrations of $Br^-$ from the electrolyte minimizes the formation of $Br_2$ during electrolysis,[67] thereby eliminating a redox-active species that further complicates the reaction mechanism and analysis. In addition, the use of di-Mebpy affords a more stable Ni complex with well-defined and readily interpretable CV behavior,[68] making it better suited for mechanistic investigations.

Figures 3b−c show that the selectivity between the desired C−N cross-coupling product and undesired C−C homocoupling product is highly sensitive to AC frequency and amplitude,


https://doi.org/10.1021/acs.accounts.6c00439
Acc. Chem. Res. XXXX, XXX, XXX−XXX

with optimal C−N coupling observed at 0.2 Hz and 3 V. To understand the AC-controlled selectivity, we first identified the major pathways leading to these two products. Specifically, the reaction proceeds through the reduction of Ni(II) (**8**) to Ni(I) (**9**), followed by oxidative addition of the aryl bromide and comproportionation to form the Ni(II)(Ar)Br intermediate (**10**). This intermediate represents a key branching point in the reaction network. From this state, three competing pathways emerge: (i) chemical decomposition to C−C product, (ii) further reduction to lower-valent Ni species (**13**) that lead to C−C homocoupling, and (iii) productive transmetalation with the amine to form **11**, ultimately yielding the desired C−N product (Figure 3d). Both (ii) and (iii) pathways are strongly dependent on electrochemical conditions, making them sensitive to AC frequency.

The central role of AC frequency becomes evident when considering the temporal evolution of intermediate **10**. Formation of this species occurs following oxidative addition, which requires a finite time ($t_{ArBr}$). If the cathodic half-cycle is too long, **10** would remain under reducing conditions and undergo further reduction to Ni(I) species that promote C−C coupling (pathway (ii)). In contrast, when the AC frequency is increased such that the cathodic duration ($t_{cathode}$) is shorter than or comparable to $t_{ArBr}$, the system switches polarity before **10** can be reduced. Therefore, when $t_{cathode} \leq t_{ArBr}$, it prevents further reduction of **10** and, instead, channels it toward transmetalation and subsequent C−N bond formation (pathway (iii) in Figure 3e). Thus, AC frequency effectively controls selectivity by limiting the exposure of the key intermediate **10** to reductive environments.

In addition to the qualitative understanding discussed above, we measured $t_{ArBr}$ using CV analysis and derived the theoretically optimal frequency for the C−N coupling reaction from the resulting data. We varied the scan rate to adjust the time available for oxidative addition and monitored the formation and subsequent reduction of **10** from the peak current values. Figures 3f−g show that at a critical scan rate of 0.2 V/s, the CV traces with and without aryl bromide overlap, indicating that oxidative addition cannot proceed within that time window. This critical time scale can be directly translated into an optimal AC frequency (∼0.3 Hz), in close agreement with the experimentally observed optimum (∼0.2 Hz). Similar analyses were performed for a series of aryl bromide substrates, and a strong correlation was observed between the optimal frequencies predicted from CVs and those determined experimentally for the C−N cross-coupling reactions. Interestingly, varying the amine coupling partner had little effect on the optimal AC frequency. This observation is consistent with the proposed mechanism, in which the frequency-determining step is the oxidative addition of the aryl bromide to the Ni(I) intermediate **9**, and the amine substrate does not participate in this elementary step.

## 4. SYNCHRONIZING HETEROGENEOUS ELECTROCATALYSIS WITH AC ELECTROLYSIS

In the previous section, we demonstrated how AC electrolysis can interact with key intermediates in a homogeneous catalytic cycle to modulate reaction selectivity. Similar principles can also be applied to heterogeneous electrocatalysis. However, heterogeneous catalytic systems are often considerably more complex than their homogeneous counterparts because they involve many surface-adsorbed intermediates, and the nature of the catalytic sites is highly heterogeneous and sometimes dynamically evolves under reaction conditions. As a result, understanding and controlling the interaction between AC electrolysis and heterogeneous catalytic processes present both unique challenges and opportunities for controlling reaction selectivity.

Through a collaboration with Corteva Agriscience, we identified a heterogeneous electrocatalytic reaction whose performance could be significantly enhanced by applying AC electrolysis. This reaction is the Ag-catalyzed dehalogenation of picloram (**14**) to yield the commercial herbicide aminopyralid (**15**), a transformation currently employed in an industrial process at Corteva (Figure 4a).[5] In the conventional process, Ag serves as the cathode and is "activated" prior to electrolysis by applying a positive voltage bias. However, a major limitation of this process is that reaction selectivity deteriorates over time, necessitating periodic interruptions to the electrolysis to reactivate the Ag catalyst.

We first reproduced this dehalogenation reaction using the industrial protocol described in the patent literature[69] and compared its performance with that obtained using a pristine Ag electrode. Consistent with industrial observations, the activated Ag electrode exhibited substantially higher catalytic activity than the untreated Ag electrode. However, the selectivity toward the desired product could not be maintained over extended reaction times. After 12 h of electrolysis, the yield of aminopyralid decreased to approximately 2%, while more than 50% of the substrate underwent decomposition. Concurrently, several side products arising from undesired dechlorination and deamination pathways, including **16**, **17**, and **18**, accumulated in the reaction mixture (Figure 4b).

We next investigated the structural evolution of the Ag catalyst during activation. We found that the "activation" procedure involves first oxidizing Ag to $Ag_2O$ and subsequently reducing $Ag_2O$ back to metallic Ag by applying a negative bias. This oxidation−reduction sequence produces a porous Ag surface enriched with defect sites, including grain boundaries, dislocations, and atomic gliding defects. However, the defect-rich Ag surface is not stable under the dehalogenation reaction conditions. During electrolysis, the activated Ag gradually reconstructs, evolving toward a more ordered structure resembling that of the pristine Ag electrode (Figure 4c). This structural relaxation is accompanied by an increase in crystallite size, as revealed by four-dimensional scanning transmission electron microscopy.

Inspired by the dynamic structural evolution of the Ag catalyst during activation and dehalogenation, we proposed using AC redox cycles to maintain its active structure and prevent irreversible degradation (Figure 4d). We optimized the reaction time, frequency, and other reaction parameters and observed a drastic improvement in the selectivity and yield of the desired product under AC conditions (Figure 4e).

In addition to maintaining the catalytic activity of the Ag catalyst, we discovered that AC electrolysis dramatically alters the chemical speciation in the reaction medium. The AC electrolysis cell employs a symmetric electrode configuration in which both electrodes are composed of Ag. As a result, the anodic reaction is dominated by the $Ag^0/Ag_2O$ redox process rather than the oxidation of $Cl^-$ to $Cl_2$. Suppressing $Cl^-$ oxidation is particularly important because $Cl_2$ readily hydrolyzes to form hypochlorite, a strong oxidant that promotes the decomposition of both the starting material and the desired product. These degradation pathways generate ammonia and, upon further oxidation, nitrite species. In turn, these reactive


https://doi.org/10.1021/acs.accounts.6c00439
Acc. Chem. Res. XXXX, XXX, XXX−XXX

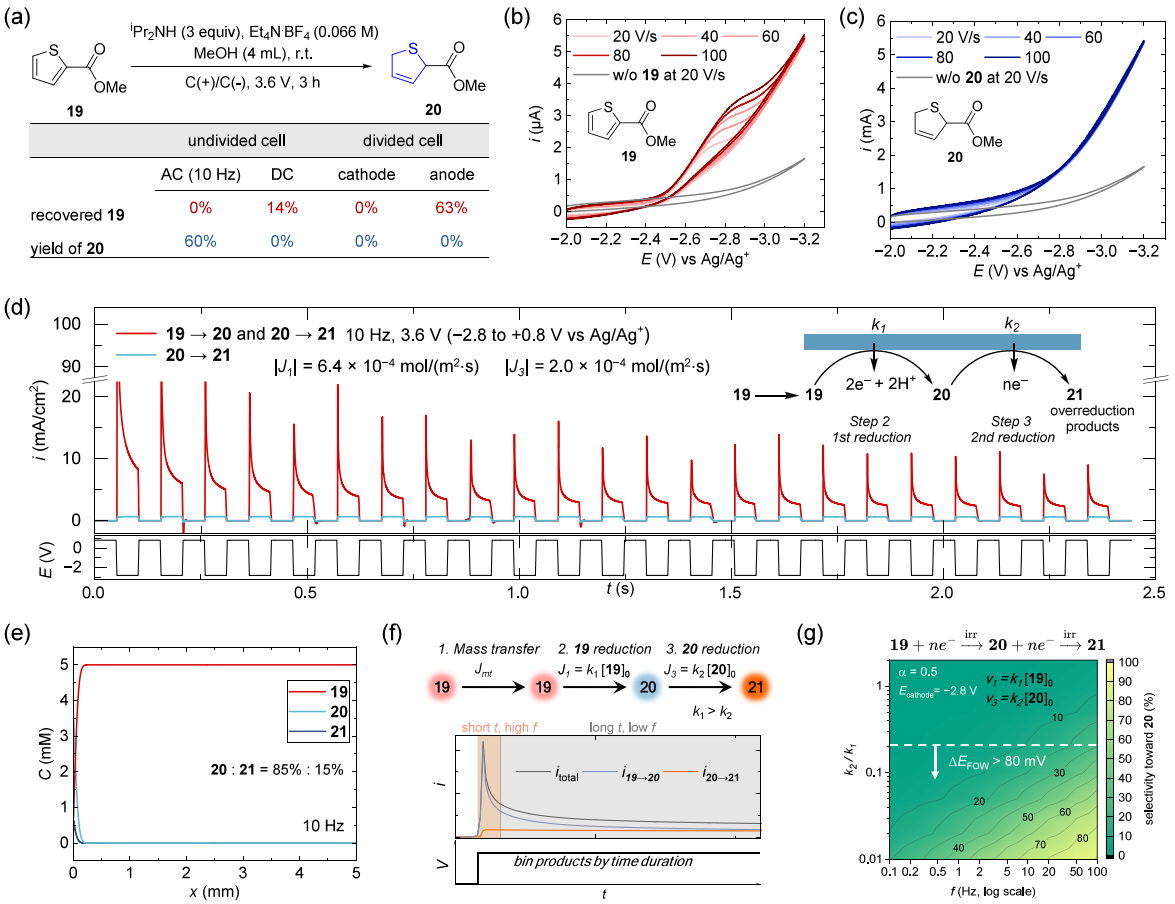


**Figure 5.** (a) Comparison of products from **19** reduction using AC electrolysis (3.6 V, 10 Hz, square wave) and DC electrolysis (3.6 V) in both divided and undivided cells. CVs of (b) 5 mM **19** and (c) 5 mM **20** in MeOH with 0.066 M TEA·$BF_4$, recorded at scan rates from 20 to 100 V/s using a carbon microdisk electrode. (d) Simulated total current for **19** → **20** → **21** and specific current for **20** → **21** at 10 Hz. (e) Simulated concentration profiles for **19**, **20**, and **21** at the end of the simulation at 10 Hz. (f) Schematic illustration showing the time-dependent evolution of the total current $i_{total}$, and the individual currents for the **19** → **20** and **20** → **21** conversions. (g) Contour plot for the yield of partial reduction product, **20**, as a function of the $k_2/k_1$ ratio and AC frequency. Reproduced with permission from ref 3. Copyright 2025 American Chemical Society.

nitrogen species can react with amino groups in the substrate and product, leading to undesired deamination. Under AC electrolysis, continuous $Ag^0/Ag_2O$ redox cycling (green pathway) effectively outcompetes $Cl^-$ oxidation, thereby shutting down $Cl_2$ formation and suppressing the subsequent decomposition and deamination pathways (grayed-out pathways in Figure 4f). As a result, the desired dehalogenation reaction proceeds with significantly improved selectivity. The AC strategy was further evaluated under long-term operating conditions to assess its robustness and practical utility. Remarkably, the reaction could be operated continuously for 50 days without any catalyst reactivation or process interruption. Throughout this period, the AC electrolysis system consistently delivered approximately 80% yield of the desired product in each batch (Figures 4g–h).

This work emphasizes an important conceptual transformation: selectivity under AC conditions results not only from the timing of intermediates (in this case, defect-rich Ag) but also from the evolution of the catalyst structure and chemical speciation during redox cycling.

## 5. INSIGHTS FROM NUMERICAL SIMULATIONS

The examples discussed thus far clearly demonstrate the power and versatility of AC electrolysis for controlling reaction selectivity. However, elucidating the origins of the observed frequency dependent behavior has required developing "customized" mechanistic analyses for each reaction system. These approaches are often highly reaction-specific and cannot be readily generalized, underscoring the need for more broadly applicable theoretical and analytical frameworks to understand, predict, and ultimately design AC-enabled reaction selectivity

As Richard Feynman famously noted, "What I cannot create, I do not understand." In the context of AC electrolysis, reproducing experimental observations through theory and simulation is therefore more than a validation exercise; it is a critical step toward uncovering the mechanistic origins of frequency-dependent selectivity and, eventually, rational design of AC-controlled reaction selectivity. This challenge motivated us to establish a finite-element modeling framework to understand frequency-dependent selectivity in AC electrolysis, as finite-element simulation can capture the complex interplay among electrochemical kinetics, mass transport, homogeneous reactions, and the dynamic redox environment characteristic of AC electrolysis.

We chose the AC-enabled selective partial reduction of (hetero)arenes, originally discovered by the Baran group,[49] as our model reaction. As shown in Figure 5a, the (hetero)arene starting material **19** mostly undergoes decomposition with 14% recovery of the starting material and no partially reduced product under DC electrolysis. In contrast, the AC electrolysis of


https://doi.org/10.1021/acs.accounts.6c00439
Acc. Chem. Res. XXXX, XXX, XXX−XXX

**19** yields a partially reduced product, **20**, in 60% yield. Control experiment in the divided-cell results show that complete decomposition occurs at the cathode, while the starting material remains intact on the anode side. This indicates that overreduction of **20** occurs in the static reducing environment of DC electrolysis, but not in the dynamic AC environment.

Although we have found that the DC conditions promote the formation of $MeO^-$ via methanol reduction, thereby promoting the base-catalyzed decomposition of **20**, the primary factor driving the AC-enabled partial reduction of **19** to **20** is still the difference in the reduction kinetics of the two species. The CVs of **19** (Figure 5b) show that its reduction is diffusion-limited, as evidenced by the linear relationship between the peak current and the square root of the scan rate. In contrast, the CVs of **20** (Figure 5c) exhibit no distinct reduction peak, indicating that its reduction is kinetically controlled, despite having a reduction onset potential similar to that of **19**.

Using the CV data, we extracted the kinetic parameters ($k_1$ and $k_2$) for the reduction of **19** and **20** and incorporated them into a finite-element model. Although the model is intentionally simplified, it captures the essential features of the reaction network, which consists of two sequential irreversible electrochemical reduction steps (**19** → **20** and **20** → **21**). Note that **21** represents all the overreduction products, rather than a particular one. Figure 5d shows the simulated total reduction current (red) together with the current specifically associated with the undesired overreduction of **20** to **21** (blue) under a 10 Hz square-wave. The relative ratio of these two currents provides a measure of the selectivity toward the desired partial reduction product, **20**; the smaller the fraction of current directed toward the second reduction step, the higher the selectivity for **20**.

Product selectivity can also be quantified directly by integrating the simulated concentration profiles of **20** and **21** over the reaction domain. Using this approach, the model predicts a product distribution of 85% **20** and 15% **21** at 10 Hz (Figure 5e). In sharp contrast, lowering the frequency to 0.1 Hz shifts the product distribution to 33% **20** and 67% **21**, indicating substantial overreduction. These simulated trends are in good agreement with the experimentally observed selectivity, demonstrating that the model successfully captures the AC-enabled partial reduction.

The finite-element model enables a convenient, quantitative analysis of the time-resolved current contributions from each reduction step for elucidating the simulated frequency-dependent selectivity. As shown in Figure 5f, upon application of a cathodic pulse, the reduction of **19** to **20** proceeds rapidly, whereas the subsequent reduction of **20** to **21** proceeds much more slowly due to its less favorable kinetics ($k_1 > k_2$). Consequently, the current associated with the first reduction step ($i_{19\rightarrow20}$) initially dominates over that of the second reduction step $i_{20\rightarrow21}$, leading to the selective formation of the partial reduction product **20**. As electrolysis continues, however, **19** near the electrode surface becomes depleted while **20** accumulates. This change gradually decreases $i_{19\rightarrow20}$ and increases $i_{20\rightarrow21}$, allowing the second reduction step to catch up. Eventually, the two currents become comparable, at which point overreduction becomes significant, and the selectivity shifts toward the fully reduced product **21**.

This model can also be readily generalized to evaluate the selectivity of any reactions involving two sequential irreversible reduction or oxidation steps under AC electrolysis conditions. Figure 5g presents a contour plot of the simulated yield of the partial reduction product **20** as a function of the kinetic ratio ($k_2/k_1$) and the AC frequency. A key insight from this analysis is that achieving synthetically useful yields of **20** (>30%) within a practical frequency range (≤100 Hz) requires $k_2/k_1 < 0.2$. In other words, the second electron-transfer step must be significantly slower than the first for AC electrolysis to effectively suppress overreduction. Because direct experimental determination of ($k_2/k_1$) is often challenging, we sought a more accessible electrochemical descriptor. We found that the foot-of-wave (FOW) potential difference ($\Delta E_{FOW}$) between the voltammograms of **19** and **20** serves as an effective proxy. In the FOW region, both reductions are under kinetic control and at sufficiently low overpotentials. Under these conditions, a kinetic ratio of $k_2/k_1 < 0.2$ corresponds to $|\Delta E_{FOW}| > 80$ mV. Consequently, $|\Delta E_{FOW}| > 80$ mV can be used as a simple experimental descriptor for assessing the feasibility of AC-enabled partial reduction.

## 6. SUMMARY AND FUTURE OUTLOOK

In summary, we have highlighted our group's recent contributions to the emerging field of AC electrolysis for organic synthesis. Using representative examples, we have shown how AC frequency can control the reactivity of amino radicals, synchronize catalytic processes in homogeneous systems, and maintain catalytically active electrode structures while altering chemical speciation in heterogeneous electrocatalysis. We have also described our initial efforts to establish finite-element modeling frameworks that provide quantitative insight into the origins of AC-enabled selectivity.

Over the past several years, AC electrolysis has gradually evolved from a seemingly "magic" black box that occasionally produces unexpected reaction outcomes into a tool whose behavior can be increasingly understood and rationalized. Nevertheless, significant challenges remain before the field's ultimate goal can be realized: the rational design of AC-enabled reaction selectivity and the quantitative prediction of reaction outcomes as a function of frequency.

From our studies thus far, AC electrolysis rarely influences only a single aspect of a reaction. Instead, it often simultaneously affects multiple interconnected processes, including electron-transfer kinetics, homogeneous reaction pathways, catalyst speciation, electrode structure, and mass transport. The complex interplay among these factors makes mechanistic interpretation challenging and predictive modeling even more difficult.

Despite these challenges, we believe that continued advances in mechanistic studies, electroanalytical methods, theoretical modeling, and data-driven approaches will accelerate the transition of AC electrolysis from an empirical optimization strategy to a predictive platform for reaction design. As our understanding deepens, AC electrolysis will become a general and powerful tool for controlling chemical reactivity through temporal modulation of the electrochemical processes. Ultimately, we envision a future in which AC-enabled reaction selectivity can be quantitatively predicted from a proposed reaction mechanism, and frequency-dependent reaction outcomes serve as mechanistic fingerprints to elucidate underlying reaction pathways.


https://doi.org/10.1021/acs.accounts.6c00439
Acc. Chem. Res. XXXX, XXX, XXX−XXX

## AUTHOR INFORMATION


### Corresponding Author

**Long Luo** − *Department of Chemistry, University of Utah, Salt Lake City, Utah 84112, United States;* orcid.org/0000-0001-5771-6892; Email: long.luo@utah.edu

### Authors

**Diptangshu Datta Mal** − *Department of Chemistry, University of Utah, Salt Lake City, Utah 84112, United States;* orcid.org/0000-0001-7584-8848

**Nibedita Behara** − *Department of Chemistry, University of Utah, Salt Lake City, Utah 84112, United States;* orcid.org/0000-0002-4278-0135

Complete contact information is available at: https://pubs.acs.org/10.1021/acs.accounts.6c00439


### Author Contributions

‡D.D.M. and N.B. contributed equally to this work.

### Notes

The authors declare no competing financial interest.

### Biographies

**Diptangshu Datta Mal** received his Ph.D. from the Indian Institute of Technology Kharagpur, India, and is currently a Postdoctoral Research Associate in the Department of Chemistry at the University of Utah. His research focuses on alternating current electrochemistry, electrosynthesis, and heterogeneous catalysis.

**Nibedita Behera** received her Ph.D. in Chemistry from the Indian Institute of Technology Guwahati, India. She is currently a Postdoctoral Research Associate in the Department of Chemistry at the University of Utah. Her research focuses on developing electrochemical strategies for hydrogen isotope labeling and electroorganic synthesis.

**Long Luo** is an Associate Professor of Chemistry at the University of Utah. He received his B.S. (2009) in Applied Chemistry from Beijing University of Aeronautics and Astronautics and his Ph.D. (2014) in Chemistry from the University of Utah under the guidance of Prof. Henry S. White. He worked as a postdoctoral fellow in the laboratory of Prof. Richard M. Crooks at the University of Texas at Austin. His laboratory explores interdisciplinary frontiers in electrochemistry.

## ACKNOWLEDGMENTS

This work was supported by NIH (1R35 GM142590), the NSF Center for Synthetic Organic Electrochemistry, CHE-2503773, the University of Utah, and the Alfred P. Sloan Foundation (Grant #FH-2023-20829). ChatGPT was used to improve the language and clarity of the manuscript during its preparation.

## REFERENCES


(1) Gunasekera, D.; Mahajan, J. P.; Wanzi, Y.; Rodrigo, S.; Liu, W.; Tan, T.; Luo, L. Controlling One- or Two-Electron Oxidation for Selective Amine Functionalization by Alternating Current Frequency. *J. Am. Chem. Soc.* **2022**, *144* (22), 9874−9882.

(2) Behera, N.; Gunasekera, D.; Mahajan, J. P.; Frimpong, J.; Liu, Z. F.; Luo, L. Electrochemical hydrogen isotope exchange of amines controlled by alternating current frequency. *Faraday Discuss.* **2023**, *247*, 45−58.

(3) Sreekumar, S.; Beeler, J. A.; Mal, D. D.; White, H. S.; Luo, L. Origin of Selectivity in Alternating Current-Enabled Partial Reduction of (Hetero)Arenes: A Case Study of Two Consecutive Irreversible Electrochemical Steps. *J. Am. Chem. Soc.* **2025**, *147* (30), 26917−26925.

(4) Hazra, A.; Organiscak, M.; Luo, L. Deciphering the Synchronization of Alternating Current Frequency with the Nickel Catalytic Cycle in Selective C-N Cross-Coupling. *J. Am. Chem. Soc.* **2025**, *147* (38), 35139−35148.

(5) Mal, D. D.; Redkar, N.; Liu, K.; Park, H.; Kennedy, E. R.; Kim, S.; Li, W.; Yang, Y.; Qi, Y.; Neurock, M.; et al. Electrosynthesis of Agrochemicals via Alternating-Current-Driven Selective, Continuous Dehalogenation. *J. Am. Chem. Soc.* **2025**, *147* (41), 37611−37621.

(6) Balcells, D.; Clot, E.; Eisenstein, O.; Nova, A.; Perrin, L. Deciphering Selectivity in Organic Reactions: A Multifaceted Problem. *Acc. Chem. Res.* **2016**, *49* (5), 1070−1078.

(7) Pradhan, T. R.; Park, J. K. Intermediate Control: Unlocking Hitherto Unknown Reactivity and Selectivity in N-Conjugated Allenes and Alkynes. *Acc. Chem. Res.* **2025**, *58* (2), 281−298.

(8) Huang, Z.; Dong, G. Site-Selectivity Control in Organic Reactions: A Quest To Differentiate Reactivity among the Same Kind of Functional Groups. *Acc. Chem. Res.* **2017**, *50* (3), 465−471.

(9) Hartwig, J. F. Catalyst-Controlled Site-Selective Bond Activation. *Acc. Chem. Res.* **2017**, *50* (3), 549−555.

(10) Afagh, N. A.; Yudin, A. K. Chemoselectivity and the curious reactivity preferences of functional groups. *Angew. Chem., Int. Ed. Engl.* **2010**, *49* (2), 262−310.

(11) Ruffoni, A.; Mykura, R. C.; Bietti, M.; Leonori, D. The interplay of polar effects in controlling the selectivity of radical reactions. *Nat. Synth.* **2022**, *1* (9), 682−695.

(12) Shen, Z.-J.; Zhu, C.; Zhang, X.; Yang, C.; Rueping, M.; Guo, L.; Xia, W. Organoboron Reagent-Controlled Selective (Deutero)-Hydrodefluorination. *Angew. Chem., Int. Ed. Engl.* **2023**, *62* (7), No. e202217244.

(13) Ye, R. P.; Ding, J.; Reina, T. R.; Duyar, M. S.; Li, H. T.; Luo, W. H.; Zhang, R. B.; Fan, M. H.; Feng, G.; Sun, J.; et al. Design of catalysts for selective CO hydrogenation. *Nature Synthesis* **2025**, *4* (3), 288−302.

(14) Xu, Y.; Li, C.; Xiao, Y.; Wu, C.; Li, Y.; Li, Y.; Han, J.; Liu, Q.; He, J. Tuning the Selectivity of Liquid Products of CO(2)RR by Cu-Ag Alloying. *ACS Appl. Mater. Interfaces* **2022**, *14* (9), 11567−11574.

(15) Elias, E. K.; Rehbein, S. M.; Neufeldt, S. R. Solvent coordination to palladium can invert the selectivity of oxidative addition. *Chem. Sci.* **2022**, *13* (6), 1618−1628.

(16) Lyons, T. W.; Hull, K. L.; Sanford, M. S. Controlling site selectivity in Pd-catalyzed oxidative cross-coupling reactions. *J. Am. Chem. Soc.* **2011**, *133* (12), 4455−4464.

(17) Ranaware, V.; Kurniawan, R. G.; Verma, D.; Kwak, S. K.; Ryu, B. C.; Kang, J. W.; Kim, J. Solvent-mediated selectivity control of furfural hydrogenation over a N-doped carbon-nanotube-supported Co/CoOx catalyst. *Appl. Catal. B* **2022**, *318*, 121838.

(18) Cainelli, G.; Galletti, P.; Giacomini, D. Solvent effects on stereoselectivity: more than just an environment. *Chem. Soc. Rev.* **2009**, *38* (4), 990−1001.

(19) Mallat, T.; Baiker, A. Selectivity enhancement in heterogeneous catalysis induced by reaction modifiers. *Appl. Catal., A* **2000**, *200* (1−2), 3−22.

(20) Liang, Y. R.; Wu, Q.; Lin, X. F. Effect of Additives on the Selectivity and Reactivity of Enzymes. *Chem. Rec* **2017**, *17* (1), 90−121.

(21) Feng, K.; Raguram, E. R.; Howard, J. R.; Peters, E.; Liu, C.; Sigman, M. S.; Buchwald, S. L. Development of a Deactivation-Resistant Dialkylbiarylphosphine Ligand for Pd-Catalyzed Arylation of Secondary Amines. *J. Am. Chem. Soc.* **2024**, *146* (39), 26609−26615.

(22) Deolka, S.; Dalmau, D.; Garcia Roca, A.; Vasylevskyi, S.; Samha, M. H.; Sigman, M. S. Development of a Heteroleptic Palladium Catalyst for the Fluorination of Arylboronic Acids using Data Science Tools. *J. Am. Chem. Soc.* **2025**, *147* (39), 35705−35717.

(23) Simlandy, A. K.; Alturaifi, T. M.; Nguyen, J. M.; Oxtoby, L. J.; Wong, Q. N.; Chen, J. S.; Liu, P.; Engle, K. M. Enantioselective Hydroalkenylation and Hydroalkynylation of Alkenes Enabled by a Transient Directing Group: Catalyst Generality through Rigidification. *Angew. Chem., Int. Ed. Engl.* **2023**, *62* (29), No. e202304013.

(24) Li, Y. H.; Ouyang, Y.; Chekshin, N.; Yu, J. Q. Pd(II)-Catalyzed Site-selective beta- and gamma-C($sp^3$)-H Arylation of Primary

Aldehydes Controlled by Transient Directing Groups. *J. Am. Chem. Soc.* **2022**, *144* (11), 4727−4733.
(25) Leech, M. C.; Lam, K. A practical guide to electrosynthesis. *Nat. Rev. Chem.* **2022**, *6* (4), 275−286.
(26) Zeng, W.; Wang, Y.; Peng, C.; Qiu, Y. Organo-mediator enabled electrochemical transformations. *Chem. Soc. Rev.* **2025**, *54* (9), 4468−4501.
(27) Leech, M. C.; Garcia, A. D.; Petti, A.; Dobbs, A. P.; Lam, K. Organic electrosynthesis: from academia to industry. *React. Chem. Eng.* **2020**, *5* (6), 977−990.
(28) Frontana-Uribe, B. A.; Little, R. D.; Ibanez, J. G.; Palma, A.; Vasquez-Medrano, R. Organic electrosynthesis: a promising green methodology in organic chemistry. *Green Chem.* **2010**, *12* (12), 2099−2119.
(29) Elsherbini, M.; Wirth, T. Electroorganic Synthesis under Flow Conditions. *Acc. Chem. Res.* **2019**, *52* (12), 3287−3296.
(30) Rafiee, M.; Mayer, M. N.; Punchihewa, B. T.; Mumau, M. R. Constant Potential and Constant Current Electrolysis: An Introduction and Comparison of Different Techniques for Organic Electrosynthesis. *J. Org. Chem.* **2021**, *86* (22), 15866−15874.
(31) Gombos, L. G.; Nikl, J.; Waldvogel, S. R. Dual Roles of Supporting Electrolytes in Organic Electrosynthesis. *ChemElectroChem* **2024**, *11* (8), e202300730.
(32) Esakki Karthik, P.; Alessandri, I.; Sengeni, A. Review—A Review on Electrodes Used in Electroorganic Synthesis and the Significance of Coupled Electrocatalytic Reactions. *J. Electrochem. Soc.* **2020**, *167* (12), 125503.
(33) Kawamata, Y.; Baran, P. S. Electrosynthesis: Sustainability Is Not Enough. *Joule* **2020**, *4* (4), 701−704.
(34) Wan, Q.; Chen, K.; Dong, X.; Ruan, X.; Yi, H.; Chen, S. Elucidating the Underlying Reactivities of Alternating Current Electrosynthesis by Time-Resolved Mapping of Short-Lived Reactive Intermediates. *Angew. Chem., Int. Ed. Engl.* **2023**, *62* (40), No. e202306460.
(35) Zeng, L.; Wang, J.; Wang, D.; Yi, H.; Lei, A. Comprehensive Comparisons between Directing and Alternating Current Electrolysis in Organic Synthesis. *Angew. Chem., Int. Ed. Engl.* **2023**, *62* (50), No. e202309620.
(36) Rodrigo, S.; Gunasekera, D.; Mahajan, J. P.; Luo, L. Alternating current electrolysis for organic synthesis. *Curr. Opin. Electrochem.* **2021**, *28*, 100712.
(37) Sattler, L. E.; Otten, C. J.; Hilt, G. Alternating Current Electrolysis for the Electrocatalytic Synthesis of Mixed Disulfide via Sulfur-Sulfur Bond Metathesis towards Dynamic Disulfide Libraries. *Chemistry* **2020**, *26* (14), 3129−3136.
(38) Fahrmann, J.; Hilt, G. Alternating Current Electrolysis as Efficient Tool for the Direct Electrochemical Oxidation of Hydroxamic Acids for Acyl Nitroso Diels-Alder Reactions. *Angew. Chem., Int. Ed. Engl.* **2021**, *60* (37), 20313−20317.
(39) Bortnikov, E. O.; Semenov, S. N. Coupling of Alternating Current to Transition-Metal Catalysis: Examples of Nickel-Catalyzed Cross-Coupling. *J. Org. Chem.* **2021**, *86* (1), 782−793.
(40) Bortnikov, E. O.; Smith, B. S.; Volochnyuk, D. M.; Semenov, S. N. Stirring-Free Scalable Electrosynthesis Enabled by Alternating Current. *Chem. Eur. J.* **2023**, *29* (18), No. e202203825.
(41) Hioki, Y.; Costantini, M.; Griffin, J.; Harper, K. C.; Merini, M. P.; Nissl, B.; Kawamata, Y.; Baran, P. S. Overcoming the limitations of Kolbe coupling with waveform-controlled electrosynthesis. *Science* **2023**, *380* (6640), 81−87.
(42) Zeng, L.; Jiao, Y.; Yan, W. S.; Wu, Y.; Wang, S. C.; Wang, P. J.; Wang, D.; Yang, Q. H.; Wang, J. X.; Zhang, H.; et al. Asymmetric-waveform alternating current-promoted silver catalysis for C-H phosphorylation. *Nat. Synth.* **2023**, *2* (2), 172−181.
(43) Wang, D.; Jiang, T.; Wan, H.; Chen, Z.; Qi, J.; Yang, A.; Huang, Z.; Yuan, Y.; Lei, A. Alternating Current Electrolysis Enabled Formal C-O/O-H Cross-Metathesis of 4-Alkoxy Anilines with Alcohols. *Angew. Chem., Int. Ed. Engl.* **2022**, *61* (18), No. e202201543.
(44) Yuan, Y.; Qi, J. C.; Wang, D. X.; Chen, Z. Y.; Wan, H.; Zhu, J. Y.; Yi, H.; Chowdhury, A. D.; Lei, A. W. Radical-Radical Cross-Coupling Assisted N-S Bond Formation Using Alternating Current Protocol. *Ccs Chemistry* **2022**, *4* (8), 2674−2685.
(45) Zeng, L.; Yang, Q.; Wang, J.; Wang, X.; Wang, P.; Wang, S.; Lv, S.; Muhammad, S.; Liu, Y.; Yi, H.; et al. Programmed alternating current optimization of Cu-catalyzed C-H bond transformations. *Science* **2024**, *385* (6705), 216−223.
(46) Feng, E. Q.; Vanswearingen, I.; Boudjelel, M.; Fabre, L.; Aldhufari, R.; Malapit, C. A. Electrochemical Oxidation of Aryl Boronic Acids via Fluoride Activation and Alternating Polarity Electrolysis for Aryl C-P Bond Formation. *ChemElectroChem* **2025**, *12* (23), No. e202500363.
(47) Fors, S. A.; Yap, Y. J.; Malapit, C. A. Effect of Alternating Polarity in Electrochemical Olefin Hydrocarboxylation. *Angew. Chem., Int. Ed. Engl.* **2025**, *64* (24), No. e202424865.
(48) Kawamata, Y.; Hayashi, K.; Carlson, E.; Shaji, S.; Waldmann, D.; Simmons, B. J.; Edwards, J. T.; Zapf, C. W.; Saito, M.; Baran, P. S. Chemoselective Electrosynthesis Using Rapid Alternating Polarity. *J. Am. Chem. Soc.* **2021**, *143* (40), 16580−16588.
(49) Hayashi, K.; Griffin, J.; Harper, K. C.; Kawamata, Y.; Baran, P. S. Chemoselective (Hetero)Arene Electroreduction Enabled by Rapid Alternating Polarity. *J. Am. Chem. Soc.* **2022**, *144* (13), 5762−5768.
(50) He, M.; Wu, Y.; Li, R.; Wang, Y.; Liu, C.; Zhang, B. Aqueous pulsed electrochemistry promotes C-N bond formation via a one-pot cascade approach. *Nat. Commun.* **2023**, *14* (1), 5088.
(51) Garrido-Castro, A. F.; Hioki, Y.; Kusumoto, Y.; Hayashi, K.; Griffin, J.; Harper, K. C.; Kawamata, Y.; Baran, P. S. Scalable Electrochemical Decarboxylative Olefination Driven by Alternating Polarity. *Angew. Chem., Int. Ed. Engl.* **2023**, *62* (42), No. e202309157.
(52) Liu, W.; Zhai, C.; Jiang, Y.; Wei, L. P.; Li, H. C.; Cai, Z. W.; Zhu, C. Applying alternating current in paired photo-electrocatalysis for asymmetric cross-coupling of alcohols. *Nat. Synth.* **2025**, *4* (12), 1534−1545.
(53) Rodrigo, S.; Um, C.; Mixdorf, J. C.; Gunasekera, D.; Nguyen, H. M.; Luo, L. Alternating Current Electrolysis for Organic Electrosynthesis: Trifluoromethylation of (Hetero)arenes. *Org. Lett.* **2020**, *22* (17), 6719−6723.
(54) De Bon, F.; Fantin, M.; Pereira, V. A.; Lourenco Bernardino, T. J.; Serra, A. C.; Matyjaszewski, K.; Coelho, J. F. J. Electrochemically Mediated Atom Transfer Radical Polymerization Driven by Alternating Current. *Angew. Chem., Int. Ed. Engl.* **2024**, *63* (29), No. e202406484.
(55) Rodrigo, S.; Hazra, A.; Mahajan, J. P.; Nguyen, H. M.; Luo, L. Overcoming the Potential Window-Limited Functional Group Compatibility by Alternating Current Electrolysis. *J. Am. Chem. Soc.* **2023**, *145* (40), 21851−21859.
(56) El Housseini, W.; Gerulskis, R.; Behera, N.; Guan, H.; Jadhav, R. G.; Nguyen, Z. A.; Baiarashov, E.; Pence, M. A.; Kamaja, V. K.; Larkin, T.; et al. Employing AC and DC Electrolysis to Modulate Electro-enzymatic Pathways for Efficient and Stereoselective H-D Exchange. *J. Am. Chem. Soc.* **2026**, *148*, 22641.
(57) Poh, Y. R.; Yuen-Zhou, J. Stirring Effects on AC-Induced Chemoselectivity in Reversible Electrochemical Reactions. *J. Phys. Chem. C* **2025**, *129* (7), 3561−3569.
(58) Poh, Y. R.; Sreekumar, S.; Luo, L.; Yuen-Zhou, J. Floquet States of Chemoselective Alternating Current Electrosynthesis. *J. Am. Chem. Soc.* **2026**, *148*, 21776.
(59) Poh, Y. R.; Kawamata, Y.; Yuen-Zhou, J. Physicochemical Principles of AC Electrosynthesis: Reversible Reactions. *J. Am. Chem. Soc.* **2024**, *146* (36), 24978−24988.
(60) Evans, J. M.; Feng, E.; Zhong, J.; Stewart, G.; Malapit, C. A. Experimental Mechanistic Studies on Alternating Polarity Electrolysis for Carbon-Centered Radical Generation. *J. Am. Chem. Soc.* **2025**, *147* (47), 43462−43473.
(61) Lennox, A. J. J.; Goes, S. L.; Webster, M. P.; Koolman, H. F.; Djuric, S. W.; Stahl, S. S. Electrochemical Aminoxyl-Mediated alpha-Cyanation of Secondary Piperidines for Pharmaceutical Building Block Diversification. *J. Am. Chem. Soc.* **2018**, *140* (36), 11227−11231.
(62) Ma, Y.; Yao, X.; Zhang, L.; Ni, P.; Cheng, R.; Ye, J. Direct Arylation of alpha-Amino C(sp(3))-H Bonds by Convergent Paired Electrolysis. *Angew. Chem., Int. Ed. Engl.* **2019**, *58* (46), 16548−16552.


https://doi.org/10.1021/acs.accounts.6c00439
*Acc. Chem. Res.* XXXX, XXX, XXX−XXX

(63) Wang, F.; Rafiee, M.; Stahl, S. S. Electrochemical Functional-Group-Tolerant Shono-type Oxidation of Cyclic Carbamates Enabled by Aminoxyl Mediators. *Angew. Chem., Int. Ed. Engl.* **2018**, *57* (22), 6686−6690.
(64) Behera, N.; Quach, N.; Maity, R.; Lehnherr, D.; Ren, S.; Li, J.; Neurock, M.; Luo, L. Alternating Current−Driven Hydrogen Isotope Labeling of Aliphatic Amines Using 1,3-Propanedithiol as an Efficient Hydrogen Atom Transfer Reagent. *J. Am. Chem. Soc.* **2026**, DOI: 10.1021/jacs.6c09099.
(65) Shetty, M.; Walton, A.; Gathmann, S. R.; Ardagh, M. A.; Gopeesingh, J.; Resasco, J.; Birol, T.; Zhang, Q.; Tsapatsis, M.; Vlachos, D. G.; et al. The Catalytic Mechanics of Dynamic Surfaces: Stimulating Methods for Promoting Catalytic Resonance. *ACS Catal.* **2020**, *10* (21), 12666−12695.
(66) Murphy, M. A.; Gathmann, S. R.; Getman, R.; Grabow, L.; Abdelrahman, O. A.; Dauenhauer, P. J. Catalytic resonance theory: the catalytic mechanics of programmable ratchets. *Chem. Sci.* **2024**, *15* (34), 13872−13888.
(67) Luo, J.; Davenport, M. T.; Callister, C.; Minteer, S. D.; Ess, D. H.; Liu, T. L. Understanding Formation and Roles of Ni(II) Aryl Amido and Ni(III) Aryl Amido Intermediates in Ni-Catalyzed Electrochemical Aryl Amination Reactions. *J. Am. Chem. Soc.* **2023**, *145* (29), 16130−16141.
(68) Tang, T.; Hazra, A.; Min, D. S.; Williams, W. L.; Jones, E.; Doyle, A. G.; Sigman, M. S. Interrogating the Mechanistic Features of Ni(I)-Mediated Aryl Iodide Oxidative Addition Using Electroanalytical and Statistical Modeling Techniques. *J. Am. Chem. Soc.* **2023**, *145* (15), 8689−8699.
(69) Wang, C.; Scortichini, C. L.; Bridson, T. S. (Dow Agrosciences LLC) Electrochemical reduction of halogenated 4-aminopicolinic acids. U.S. Patent US7666293B2, 2010.




https://doi.org/10.1021/acs.accounts.6c00439
*Acc. Chem. Res.* XXXX, XXX, XXX−XXX